ACS Biomaterials SCIENCE & ENGINEERING

Article

Cite This: ACS Biomater. Sci. Eng. 2018, 4, 1037−1045

Nanoladders Facilitate Directional Axonal Outgrowth and Regeneration

Yimin Huang,[†,¶] Ying Jiang,[§,¶] Qiuyu Wu,[∥] Xiangbing Wu,[⊥] Xingda An,[†] Alexander A. Chubykin,[∥] Ji-Xin Cheng,[*,†,‡,§] Xiao-Ming Xu,[*,⊥] and Chen Yang[*,†,‡]

[†]Department of Chemistry, Boston University, 590 Commonwealth Avenue, Boston, Massachusetts 02215, United States

[‡]Department of Electrical and Computer Engineering, Boston University, 8 St Mary's Street, Boston, Massachusetts 02215, United States

[§]Department of Biomedical Engineering, Boston University, 44 Cummington Mall, Boston, Massachusetts 02215, United States

[∥]Department of Biological Sciences, Purdue University, 915 W. State Street, West Lafayette, Indiana 47907, United States

[⊥]Stark Neurosciences Research Institute, Indiana University School of Medicine, 320 W. 15th Street, Indianapolis, Indiana 46202, United States

Supporting Information

ABSTRACT: After injuries, axonal regeneration over long distance is challenging due to lack of orientation guidance. Biocompatible scaffolds have been used to mimic the native organization of axons to guide and facilitate axonal regeneration. Those scaffolds are of great importance in achieving functional connections of the nervous system. We have developed a nanoladder scaffold to guide directional outgrowth and facilitate regeneration of axons. The nanoladders, composed of micron-scale stripes and nanoscale protrusions, were fabricated on the glass substrate using photolithography and reactive ion etching methods. Embryonic neurons cultured on the nanoladder scaffold showed significant neurite elongation and axonal alignment in parallel with the nanoladder direction. Furthermore, the nanoladders promoted axonal regeneration and functional connection between organotypic spinal cord slices over 1 mm apart. Multimodality imaging studies revealed that such neuronal regeneration was supported by directional outgrowth of glial cells along nanoladders in the organotypic spinal cord slice culture as well as in the coculture of glial cells and neurons. These results collectively herald the potential of our nanoladder scaffold in facilitating and guiding neuronal development and functional restoration.

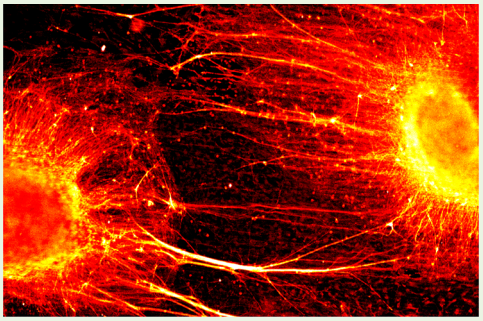

KEYWORDS: *nanobio interfaces, directional outgrowth, neuron regeneration, functional reconnection*

1. INTRODUCTION

Neurons are naturally encompassed by a network in a highly aligned manner.[1] During neuronal development, directional outgrowth is of great importance in guiding neurites to the targets, such as postsynaptic neurons, for effective communication.[2,3] Limited neuronal regeneration following central nervous system damage poses significant challenges for the treatment of injuries.[4,5] Nanostructures, *partially* mimicking the structure of the extracellular matrix, have shown potential in facilitating neurite outgrowth as well as regeneration. Uniaxially aligned nanofiber arrays with a fiber diameter of 250 nm and length in the range from 500 μm to 1 mm were applied to direct and enhance axonal extension during regeneration.[6] Nanogroove structures with feature size ranged from 50 to 600 nm fabricated on various substrates were shown to control neurites alignment of the neuronal cells cultured on the surface.[7] Arrays of nanopillars with diameters of approximately 150 nm and heights of several μm in close contact with neurons significantly reduced cell mobility and pinned the neuronal cells to the pillars to grow.[8] Nanowires with diameters of 72 ± 8 nm, lengths of 7 to 10 μm, and density of 17.9 nanowires/μm^2 were found to promote the growth of single and elongated major neurites via axon-first neurogenesis.[9] All of these studies only focused on understanding the neurite outgrowth at the cellular level, where no functional performances were measured or evaluated. Very recently, carbon nanotubes were demonstrated to increase neuronal electrical signaling.[10] Meshes of randomly distributed carbon nanotubes promoted physiological reconnections between segregated spinal cord slices placed at a distance between 300 to 800 μm.[11] Notably, the meshed carbon nanotube scaffolds lack controlled alignment of nanostructures to facilitate directional neurite regeneration. Therefore, it remains challenging to achieve regeneration and reconnection over longer distances, such as above 1 mm, a critical gap that injured lesion sites typically have in the clinical cases.[12]

Received: December 14, 2017
Accepted: February 17, 2018
Published: February 17, 2018

DOI: 10.1021/acsbiomaterials.7b00981
ACS Biomater. Sci. Eng. 2018, 4, 1037−1045

Here, we report a nanoladder scaffold that is able to guide millimeter-scale neural growth along predefined directions and to promote neurite elongation through nanostructures with a subcellular dimension. We use SiO_2-based cover glasses as the substrate to fabricate nanoladder structures, via robust photolithography and reactive ion etching (RIE) methods.[13,14]

This substrate provides high biocompatibility for neural adhesion and transparency for optical imaging to explore the growth mechanism. To evaluate the concept of nanoladder-mediated growth and regeneration, we first cultured primary embryonic neurons on the nanoladders to verify that nanoladders can guide directional outgrowth of axons. Then, using organotypic spinal cord slices placed 1 to 1.5 mm apart as an *ex vivo* injury model,[15] we showed that nanoladders promote axonal regeneration and functional connection after injuries. Furthermore, we explored the outgrowth mechanism using various imaging modalities, including immunofluorescence, scanning electron microscopy (SEM), and stimulated Raman scattering (SRS) microscopy. Detailed results are shown below.

2. EXPERIMENTAL SECTION

2.1. Materials. The photoresist AZ9260 and AZ400 K developer were purchased from AZ Electronic Materials, NJ. Polystyrene beads with the diameter of 500 nm, poly-D-lysine, penicillin/streptomycin, bovine serum albumin (BSA), Triton X-100, OsO_4, strychnine and bicuculline were purchased from Sigma-Aldrich Chemical Co, MO. Glutamine-Dulbecco's Modified Eagle Medium (DMEM), neurobasal medium, B27, N2, glutamine, anti-MAP2, anti-Tau, anti-chicken secondary antibody, and goat anti-mouse antibody were purchased from Thermo Fisher Scientific Inc., MA. Trypsin/ehylenediaminetetraacetic acid (EDTA) and phosphate-buffered saline (PBS) were purchased from VWR, PA. Fetal bovine serum (FBS) and horse serum (HS) were purchased from Atlanta Biologicals, GA. All other chemicals were purchased from Sigma-Aldrich or Dot Scientific and used without further purification.

2.2. Methods. *2.2.1. Fabrication and Characterization of Nanoladder Scaffolds.* All fabrications were carried out in the clean room in Birck Nanotechnology Center at Purdue University (West Lafayette, IN, United States). Cover glasses (22 mm × 22 mm, VWR, PA) were used as the substrates in nanoladder fabrication. The cover glasses were cleaned through multiple steps of solvent rinse, in the sequence of toluene, acetone, isopropanol, and deionized water before the photolithography process. During the photolithography, photoresist AZ9260 (AZ Electronic Materials, NJ) was spin-coated onto the cover glasses, at a speed of 2000 rpm/s for 50 s to get a thickness around 10 μm. After the cover glass substrates were soft-baked at 110 °C for 180 s, they were exposed to UV light by using a mask aligner (MA6, Suss) with an exposure power of 14.0 mW for 81 s. The developing process was carried out by applying AZ400 K developer (AZ Electronic Materials, NJ) diluted with deionized water to a ratio of 1:3. Then, the micronstripes were fabricated onto the cover glasses substrates via RIE (STS-AOE DRIE). During the etching process, a pressure of 4 mTorr and the constant CF_4 gas flow at 14 sccm were used. The radio frequency (RF) power was set at 400 W and bias power was 50 W for the entire etching process. The substrates were etched for 25 min to reach the etching depth of 10 μm. The substrates were sonicated in acetone solvent for 10 min to remove the photoresist residues. Afterward, the nanoprotrusions were fabricated onto the micronstripes. Polystyrene beads with the diameter of 500 nm (Sigma-Aldrich, MO) were deposited to the prepared micronstripe substrates with a spin coating speed of 2000 rpm/s for 45 s and used as the etching mask. The same etching process was utilized for the nanoprotrusions with a decrease etching time for 3 min. Nanoladder scaffolds were obtained after the acetone rinse to remove the unreacted polystyrene beads.

2.2.2. Animals. Embryonic day (E) 14−15 rats, obtained from female, pregnant Sprague−Dawley rats bred were used. All animal care was carried out in accordance with the National Institute of Health Guide for the Care and Use of Laboratory Animals (NIH Publications No. 80−23; revised 1996) and was operated under protocol 1406001097 approved by Purdue University Animal Care and Use Committee, and protocol 000197 approved by Boston University Animal Care and Use Committee.

2.2.3. Spinal Cord Primary Neuron Culture and Neuron-Glial Coculture. All substrates used in the embryonic neuron cell cultures were immersed in 0.01% Poly- D-Lysine (Sigma-Aldrich, MO) for overnight at 4 °C and washed in PBS before culture initiation. Primary spinal cord neurons were obtained from Sprague−Dawley rat E15 embryos. The spinal cords were isolated and placed in the L15 medium. Meninges were removed and spinal cords were cut into small pieces, dissociated by incubation in 0.05% trypsin/ethylenediaminetetraacetic acid (EDTA, VWR, PA) 15 min at 37 °C and triturated every 5 min. Dissociated cells were washed with and triturated in 10% heat-inactivated fetal bovine serum (FBS, Atlanta Biologicals, GA), 5% heat-inactivated horse serum (HS, Atlanta Biologicals, GA), 2 mM Glutamine-Dulbecco's Modified Eagle Medium (DMEM, Thermo Fisher Scientific Inc., MA), and cultured in cell culture dishes (100 mm diameter) for 30 min at 37 °C to eliminate glial cells and fibroblasts. The supernatant containing neurons was collected and seeded on poly-D-lysine coated cover glass and incubated in a humidified atmosphere containing 5% CO_2 at 37 °C with 10% FBS + 5% HS + 2 mM glutamine DMEM. After 16 h, the medium was replaced with Neurobasal medium (Thermo Fisher Scientific Inc., MA) containing 2% B27 (Thermo Fisher Scientific Inc., MA), 1% N2 (Thermo Fisher Scientific Inc., MA), and 2 mM glutamine (Thermo Fisher Scientific Inc., MA).

For neuron-glial coculture, glial cells were obtained from P2-4 rat pup cortices. Glial cells were seeded onto the substrates without coating and were cultured with DMEM + 10% FBS + 1% penicillin/streptomycin (Sigma-Aldrich, MO) for 1 week before the E14 spinal cord neurons were seeded. All cells were incubated at 37 °C in a 5% CO_2 atmosphere.

2.2.4. Immunofluorescence Staining. To track neurite outgrowth, cells were fixed with 4% paraformaldehyde for 20 min. After 3 washes, cells were blocked in 5% bovine serum albumin (Sigma-Aldrich, MO) for 30 min and permeabilized with 0.2% Triton X-100 (Sigma-Aldrich, MO). Then cells were incubated with chicken monoclonal anti-MAP2 (1:1000) and mouse monoclonal anti-Tau (1:1000) antibody for 2 h, and then with goat anti-chicken secondary antibody (1:1000, Thermo Fisher Scientific Inc., MA) or goat anti-mouse antibody (1:1000, Thermo Fisher Scientific Inc., MA) for 1 h at room temperature.

2.2.5. Scanning Electron Microscopy. Cells were fixed in glutaraldehyde solution and then rinsed three times in phosphate-buffered saline (PBS, VWR, PA). Subsequently, samples were immersed in OsO_4 (Sigma-Aldrich, MO) for 40 min and then rinsed 3 times in PBS, followed by dehydration. The dried samples were mounted on aluminum stubs and coated with platinum for imaging.

2.2.6. Organotypic Spinal Cord Slice Culture. Spinal cords or cortex from Rat E15 embryos were isolated and sliced into slices in the thickness of 250 μm with a tissue slicer. Slices were then placed on nanoladders or cover glasses. Organotypic slices were cultured with 1 mL of medium containing 67% DMEM, 8% sterile water, 25% fetal bovine serum, and 25 ng/mL nerve growth factor; adjusted to 300 mOsm and pH 7.35; and incubated in a humidified atmosphere containing 5% CO_2 at 37 °C for 7 to 14 days before fixation, staining, and imaging.

2.2.7. Stimulated Raman Scattering (SRS) Microscopy. SRS images were obtained as previously described.[16] For each SRS image, the Z position of the focus was adjusted near the equatorial plane of the neurons so that the soma and neurites were both clearly visualized. The pump (799 nm) and Stokes (1040 nm) powers before the microscope were maintained at 20 and 100 mW, respectively. Both pump and Stokes beams were linearly polarized. No cell or tissue damage was observed. Images were acquired at 2 μs pixel dwell time.

2.2.8. Electrophysiology. Electrophysiological recordings were conducted at room temperature in normal Krebs solution containing (mM): NaCl, 156; KCl, 4; $MgCl_2$, 1; $CaCl_2$, 2; Hepes, 10; glucose, 10

DOI: 10.1021/acsbiomaterials.7b00981
ACS Biomater. Sci. Eng. 2018, 4, 1037−1045

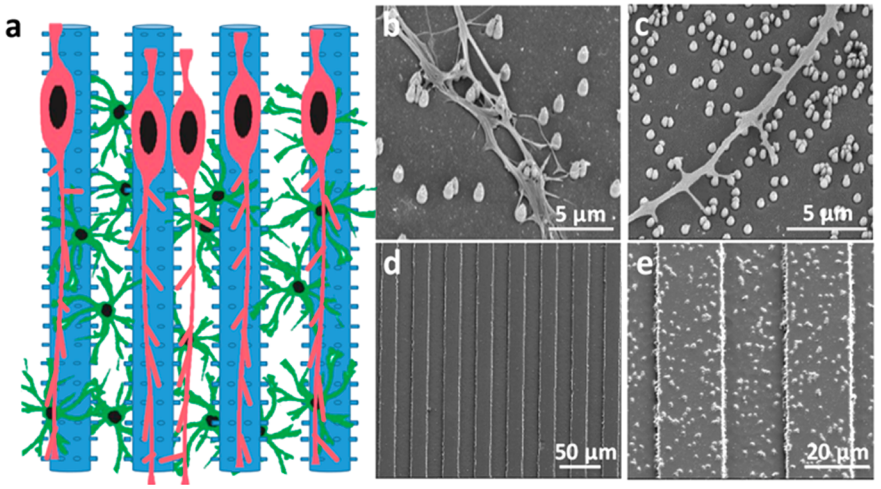

Figure 1. Concept and characterization of the nanoladder scaffold. (a) Schematic of a nanoladder scaffold (blue) mimicking the multiscale extracellular structure of the spinal cord. Red and green represent neurons and glial cells, respectively. (b,c) Embryonic neurons cultured on the silicon wafer with a low density (b) and high density (c) of nanoprotrusions, respectively. (d,e) Top view SEM images of micronstripes (d) and nanoladders scaffold (e).

(Dot Scientific, MI). Disinhibited rhythmic bursts were obtained by bath coapplication of strychnine and bicuculline (1 μM and 20 μM, respectively, Sigma-Aldrich, MO). The pH was adjusted to 7.4 using NaOH. Glass pipettes used for recording local field potentials were pulled from filamented borosilicate glass capillaries (BF150-86-10, Sutter Instruments) using a micropipette puller (Sutter Instruments, P-97), 0.8 to 1.5 MΩ resistance, and filled with normal Krebs solution. Electrical signals were amplified with MultiClamp 700B amplifier (Molecular Devices) and digitized by Digidata 1550 (Molecular Devices). Electrical stimulation was performed using a stimulus isolator (World Precision Instruments) and applied through a bipolar stimulating electrode (FHC). The stimulating current was set at 1.7 nA for all recordings. The recording results were analyzed through NEO 0.3.3 (Github), a package for representing electrophysiology data in Python. A low pass filter (cutoff frequency = 0.2 Hz) was applied to denoise the recording signals.[17]

3. RESULTS

Distinct from other nanostructures reported, the nanoladder is composed of micrometer-wide stripes and nanometer-scale protrusions on each stripe (Figure 1a). As a combination of two scales, the nanoladder structure is unique in that it highly mimics the native structure of the axonal bundles in spinal cord white matter. The micrometer-wide stripes provide directional guidance to the growing neurons and glial cells. Meanwhile, the nanoscale protrusions on each stripe serve as topographical cues to trigger neurite outgrowth and regeneration.

3.1. Fabrication and Characterization of Nanoladder Scaffolds. During neuronal development or regeneration after injury, axons outgrow to reach their targets and form functional connections.[5,18] We first investigated the efficacy of using nanoprotrusions as mechanical cues to facilitate neurite outgrowth. Nanoprotrusions of diameters of 250 and 500 nm and heights in the range of 1.0 to 2.5 μm were fabricated on silicon wafers via RIE methods. SiO_2 nanoparticles with the diameters of 250 and 500 nm (Sigma-Aldrich, MO) were used as etching masks. Silicon wafers were chosen here because it is the most commonly used substrate in nanostructure fabrication. As reported before,[19] diameters of the resulted nanoprotrusions were determined by the size of SiO_2 nanoparticles and the height was controlled by the RIE etching time. The density of nanoprotrusions on the surface was varied by changing the concentration of SiO_2 nanoparticle solution. Embryonic neurons were cultured on the poly-D-lysine (Sigma-Aldrich, MO) precoated surface of the nanoprotrusions for 7 days. Among the various dimensions we tested, more elongated neurites were found on the nanoprotrusions with 500 nm in diameter and 2 μm in height (SI Figure S1). Therefore, nanoprotrusions of such dimensions were used through the rest of our study.

To examine nanoscale details of neurite growth, we fixed the neurons for SEM imaging. We noticed that the growth pattern of neurons varied as the nanoprotrusions density changed. Specifically, when the concentration of SiO_2 nanoparticle solution used was 0.5 mg/mL and the resulted density of nanoprotrusion was $(0.17 \pm 0.06) \times 10^8$ cm^{-2}, outgrowing neurites tended to grow in the spaces between the nanoprotrusions and wrap around the protrusions as anchoring positions for further expansion (Figure 1b). As the concentration of the SiO_2 nanoparticle solution increased to 1.0 mg/mL, which resulted in a higher estimated density of $(0.80 \pm 0.14) \times 10^8$ cm^{-2} (Figure 1c), a single neurite with elongated length was observed. Interestingly, consistent with the previous report, neurites are prone to attach to the tip of the nanoprotrusions to grab and climb following the course of the nanoprotrusions.[9] These findings suggest that the nanoprotrusions offer mechanical cues to the neurite outgrowth, with nanoprotrusion dimension and density being the important parameters affecting the growth behaviors of the neurite.

To enable directional outgrowth of neurites, we utilized the aforementioned nanoladder concept (Figure 1a). Nanoladder scaffolds were fabricated on the SiO_2 based cover glass via photolithography and two-steps of RIE, as illustrated in SI Figure S2. The cover glass is chosen here because of its low price, high biocompatibility and excellent transparency for the convenience of optical imaging. A layer of photoresist (PR) AZ9260 (AZ Electronic Materials, NJ) with the thickness of approximately 10 μm was first spin-coated onto the cover glass, followed by a photolithography process to obtain the micrometer-wide stripe patterns on the PR layer. The first step of RIE was performed using CF_4 gas as the reactant, providing an etching rate of 290 nm/min for the glass and

DOI: 10.1021/acsbiomaterials.7b00981
ACS Biomater. Sci. Eng. 2018, 4, 1037−1045

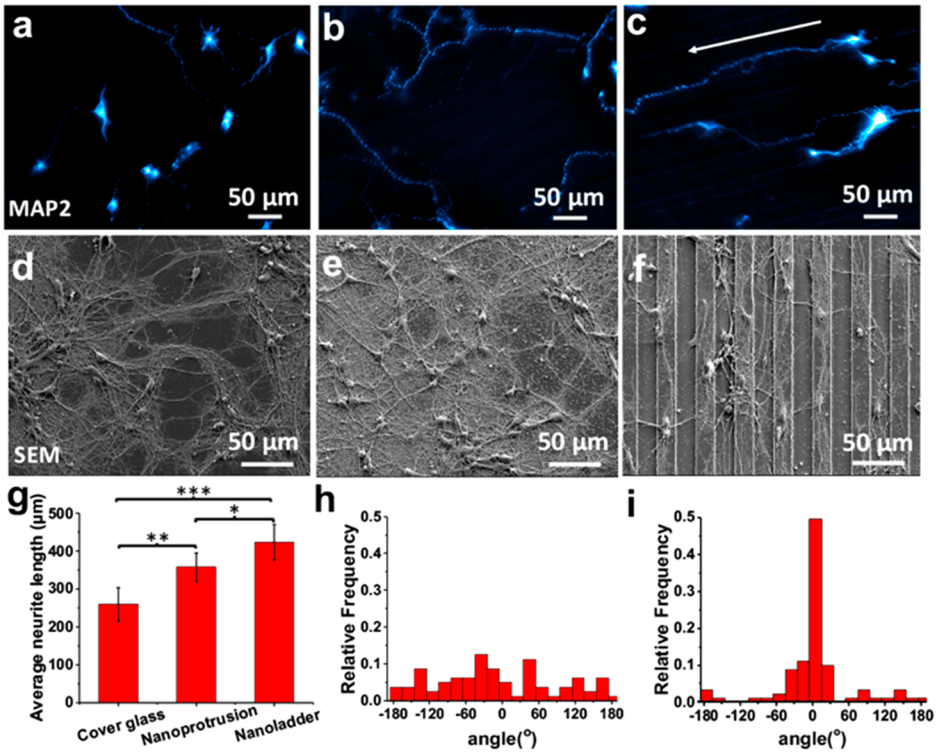

Figure 2. Nanoladders enable directional outgrowth of cultured embryonic neurons. (a–c) Immunofluorescence staining images of embryonic neuron cells cultured on the surface of different scaffolds. MAP2 stained embryonic neuron cells cultured on the cover glass (a), on nanoprotrusions (b), and on nanoladder scaffolds (c). The arrow indicates the direction of nanoladder scaffold. (d–f) SEM images of neuron cells cultured on the cover glass (d), on nanoprotrusion (e), and on nanoladder scaffolds (f). (g) Average neurite lengths measured from the immunofluorescence staining images. (h,i) Histograms of neurite angles measured from the cover glass sample (h) and nanoladder scaffold sample (i). *: $p < 0.5$; **: $p < 0.01$; ***: $p < 0.001$.

194.4 nm/min for PR, which corresponded to a selectivity of 1:1.49 (PR/glass). The stripe pattern with a width of 20 μm and a spacing of 20 μm between each stripe was therefore successfully fabricated onto the cover glass (Figure 1d). Patterns with other dimensions, including 20 μm width and 50 μm spacing, 20 μm width and 100 μm spacing, and 10 μm width and 5 μm spacing, respectively, were also designed and fabricated based on the same photolithography process (SI Figure S3a–d). Among all tested stripes, only the ones with 20 μm width and 20 μm spacing showed directional growth of neurites after culturing with embryonic spinal cord neurons. We attributed this intriguing selectivity to the fact that 20 μm is the most comparable size with the neuronal soma, which allows neurons to stay on the top and/or side of the stripes to provide optimal guidance for the neurite outgrowth (SI Figure S3e–h).[20] Afterward, the nanoprotrusions on the micronstripes were obtained by a second step of the RIE process, using polystyrene beads (Sigma-Aldrich, MO) with the diameter of 500 nm as the mask (Figure 1e). As indicated in the cross-sectional SEM images in SI Figure S4, the height of the stripes of the nanoladder scaffold is 5.40 ± 0.28 μm (SI Figure S4a) and the height of the nanoprotrusions is 2.08 ± 0.23 μm (SI Figure S4b).

3.2. Nanoladders Facilitate Directional Neurite Outgrowth and Axonal Elongation. To evaluate the interaction between neurons and the nanoladder scaffolds, we harvested embryonic spinal cord neurons from E14-E15 Sprague–Dawley rat (Charles River, MA) embryos and seeded them onto the nanoladder scaffolds. After 7 days in culture, cell growth was assessed by optical imaging and electron microscopy (Figure 2). We compared three different substrates as scaffolds for neuronal cultures, including cover glass as a control (Figure 2a,d), cover glass with only nanoprotrusions (Figure 2b,e), and nanoladders (Figure 2c,f). To visualize the dendrite outgrowth, we stained the cells with anti-MAP2 (Sigma-Aldrich, MO) for dendrites (Figure 2a–c). Neurons cultured on the nanoprotrusions showed a significant dendrite elongation (Figure 2b), compared with those in the control group (Figure 2a). Significantly, in the nanoladder group, a directional neurite elongation along the orientation of the nanoladders was observed (Figure 2c). We further used SEM to visualize more detailed neurite structures. In the control group (Figure 2d), the neurites tended to aggregate into bundles, while neurons in the nanoprotrusion group showed a more spread out and expanded growth pattern (Figure 2e). In the nanoladder group, neurites were noticeably guided by the nanoladder and followed the orientation of nanoladders (Figure 2f).

Quantitative analysis of the neurite elongation and orientation was performed on the basis of the immunofluorescence images. The neurite elongation was determined by measuring the average neurite length in the ImageJ via NeurphologyJ plugins. As displayed in Figure 2g, the average total neurite lengths per neuron are 259.91 ± 19.94 μm (n = 31), 358.46 ± 16.69 μm (n = 24), and 424.05 ± 19.35 μm (n = 22) for the control, nanoprotrusions, and nanoladder groups, respectively. The neurite lengths observed from nanoprotrusions and nanoladder groups are significantly longer than that of the control group, $p = 0.0053$ for the nanoprotrusion versus cover glass group and $p = 2.37 \times 10^{-4}$ for the nanoladder versus

DOI: 10.1021/acsbiomaterials.7b00981
ACS Biomater. Sci. Eng. 2018, 4, 1037–1045

cover glass group, respectively. These results indicate that nanoprotrusions effectively promote the neurite outgrowth.

The orientation of the neurites was determined by measuring the angle between the primary neurites and nanoladder orientations. (Figure 2h,i). In the control group, embryonic neuron cells displayed a uniform distribution over a broad range of orientation angles in the degree of −180° to 180°, with 27.5% of the neurite orientation within the angle of −30° to 30° (n = 91). On the contrary, the majority of the neuron cells on the nanoladder group were aligned in parallel to the orientation of the nanoladders, with 79.12% of the neurite orientation within the −30° to 30° range (n = 80). This comparison demonstrates that nanoladders predefine a specific direction and effectively facilitate the directional neurite outgrowth along the direction.

Because axonal elongation is important for the formation of functional synapses, we further stained with anti-Tau antibodies (Sigma-Aldrich, MO) to specifically label axons. Figure 3a−c shows that the average axonal lengths are 125.22 ± 13.02 (n = 20), 165.67 ± 10.57 (n = 37), and 231.35 ± 17.69 (n = 30) μm for the control, nanoprotrusions, and nanoladder groups, respectively. As shown in Figure 3d, the directional axonal length in the nanoladder group (blue) is significantly longer (p = 2.02 × 10^{-4}) than the axonal length in the control group (black), which is consistent with the dendrite growth results obtained from MAP2 staining. In addition, axons on nanoladder scaffold also follow the direction of the micronstripes (arrow shown in Figure 3c). Collectively, these results confirm that the nanoladder scaffold promotes the directional growth of dendrites as well as axons from embryonic neurons.

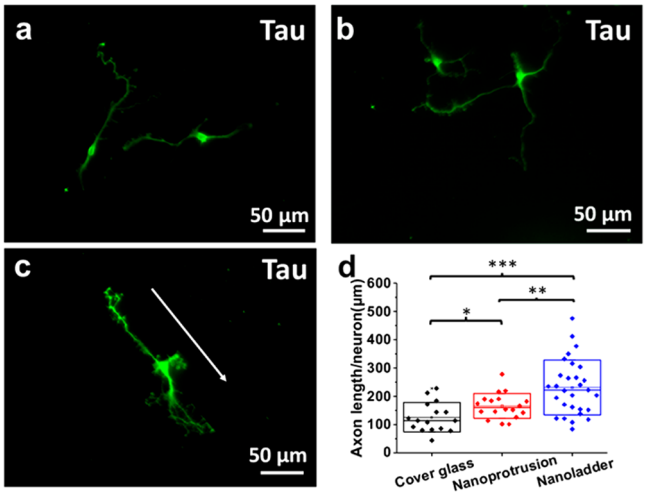

Figure 3. Axonal elongation of embryonic neurons cultured on the nanoladder scaffold confirmed using anti-Tau as the axon marker. Anti-Tau antibody stained embryonic neuron cells cultured on the cover glass (a), on nanoprotrusions (b), and on nanoladder scaffolds (c). The arrow indicates the direction of nanoladder scaffold. (d) Analysis of axonal lengths measured. *: p < 0.5; **: p < 0.01; ***: p < 0.001.

3.3. Nanoladder Scaffold Facilitates Regeneration and Reconnection in Segregated Spinal Slices. Because nanoladders can successfully guide the neurite growth of embryonic neurons, we then evaluated the potential of the nanoladder scaffolds in facilitating and, more importantly, directing neurite regeneration after injuries. We used organotypic spinal cord cultures as a simplified model for injured neurons.[21] We first characterized the growth pattern of individual slice cultured on two different substrates: the cover glass as a control group and the nanoladder group. Slices with 250 μm thickness were extracted from the E15 rat embryonic spinal cord and seeded onto the substrates. After culture for 10 days, we used anti-SMI31 (EMD Millipore, MA) to stain neurofilament to characterize regenerating axon bundles. As shown in Figure 4a,b, the slices exhibited outgrowth of axonal fibers in both groups. However, the growth manners were significantly different. In the control group, we found random outgrowth of neuronal fibers in all directions, which formed an interconnected mesh with limited expansion. In contrast, the nanoladder scaffold guided the directional growth and expansion of the regenerating axons. We also quantified the maximal regenerating axon length by manually choosing the center of slices as the starting point and measuring the distance between the starting point to the end of the longest axons expansion. As shown in Figure 4c, the average maximal regenerating axon expansion in the nanoladder group was found to be 1872 ± 464 μm (n = 10 slices), exceeding 1 mm length, and 2.59 times longer than the average expansion of 721 ± 241 μm (n = 8 slices) measured in the control group (p = 2.54 × 10^{-6}). These results suggest that the nanoladder scaffolds facilitate axonal regeneration from a single spinal slice and further expansion in a predefined direction.

Furthermore, to evaluate whether nanoladder scaffolds can promote neuronal reconnection after injury, we placed slices in pairs at a distance of 1.0 to 1.5 mm. Such distance is known to impair functional reconnection under normal conditions[22] and provides an opportunity to test if the nanoladder could meet the clinical needs. After culture for 10 days, the slices were fixed and stained with SMI31. On the cover glass (Figure 4d), slice pairs showed a similar interconnected mesh pattern as previously seen in single slices, with no visible connection between the slice pairs. By comparison, in the nanoladder group (Figure 4e), with the pair of the slices placed parallel to the orientation of the nanoladder, the regenerating axons followed the guidance of the nanoladder and morphologically connected onto the other slice. Our data suggest that the directional outgrowth of axons on the nanoladder scaffold efficiently promotes the neuronal network reconnection over a distance longer than 1 mm in the organotypic spinal cord slice model.

3.4. Electrophysiology Recordings Confirm Functional Reconnection between Spinal Cord Slices. The observed morphological connections set the basis of synaptic connection. Thus, we asked whether the nanoladder scaffold promoted functional connections between the slices. The experiment design is shown in the Figure 5a,b. The slices were cultured on either cover glass or the nanoladder scaffold. Slice pairs with a separation distance of 1.0 to 1.5 mm, measured from differential interference contrast images, were selected for recording. We used a stimulation electrode to stimulate the left slice of a chosen pair and performed local field potential recordings on both left and right slices simultaneously. To characterize the stimulated response, we delivered four 0.2 ms, 170 nA current stimulation at an interval of 0.5 s to the left slice. In both control and nanoladder groups, the stimulated slice showed robust evoked potential (black curves in Figure 5c,d). As shown in the representative trace of the local field potential recordings, the unstimulated slice on the right side of the control group showed no detectable response to the stimulation on the left slice (red curve in Figure 5c). In

DOI: 10.1021/acsbiomaterials.7b00981
ACS Biomater. Sci. Eng. 2018, 4, 1037−1045

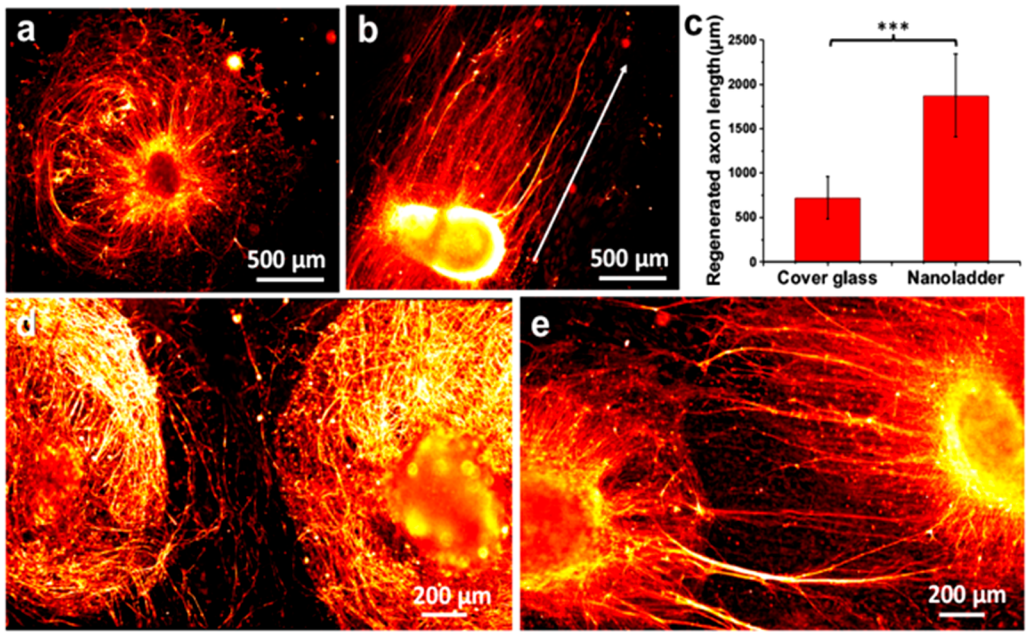

Figure 4. Nanoladders facilitate regeneration and neuronal network reconnection between organotypic spinal cord slices. (a,b) Immunofluorescence staining images of the spinal cord tissue slices cultured on the cover glass as a control group (a) and on nanoladder scaffolds (b), respectively. The arrow shows the direction of nanoladder scaffold. (c) Data analysis of the maximum regenerated axonal lengths of the control and nanoladder groups. (d,e) Immunofluorescence staining images of a pair of the spinal cord tissue slices cultured on the cover glass (d) and on nanoladder scaffolds (e), respectively. ***: $p < 0.001$.

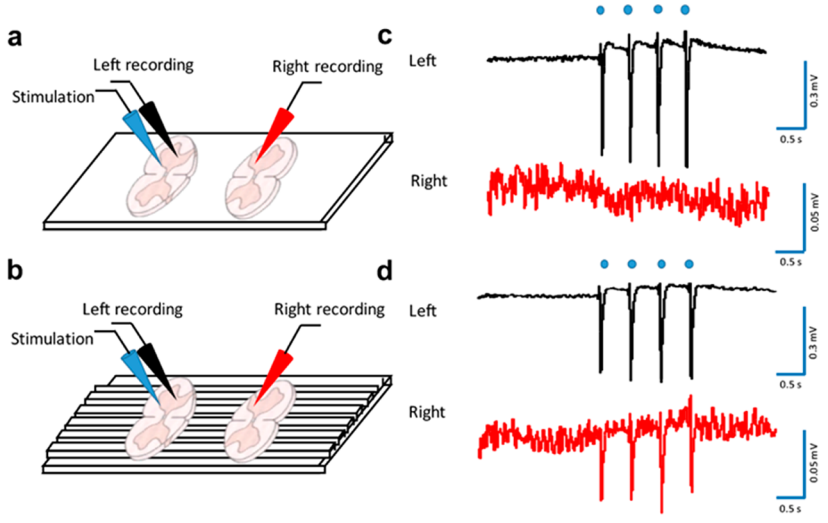

Figure 5. Electrophysiology confirms restoration of neuronal connection. Local field potential measured from embryonic spinal cord slice pairs cultured on the cover glass and on the nanoladder scaffolds, respectively. (a,b) Schematic of the experimental setting for dorsal stimulation. (c,d) Bursting local field potential entrainment by dorsal electrical stimulation of a pair of spinal cord slices on the control (c) and nanoladder scaffolds (d). Dots represent the onset of each burst.

contrast, in a representative trace of the nanoladder group, the unstimulated slice displayed evoked potential to the stimulation (red curve in Figure 5d), indicating that the slices had regenerated axons synapsing with each other and formed active connections that supported the propagation of electric signals. In addition, we observed a similar electrical response when the position of the stimulator was switched from the left slice to the right one (SI Figure S5), which further confirmed the functional connection between the pair of the slices. Collectively, our data support that nanoladder scaffold facilitates functional connections in injured sliced along a predefined direction over a distance longer than 1 mm.

3.5. Neuronal Regeneration on the Nanoladder Scaffold Is Supported by Directional Growth of Glial Cells. In the spinal cord tissue cultures, multiple types of cells are present, including neuron cells and glial cells.[23,24] Glial cells play a major role in supporting the growth and signal transduction of axon bundles. Toward understanding the mechanism behind the interactions between the nanostructures to the neuronal cells, we explored how glial cells in the organotypic slice culture can contribute to the formation of functional connections on the nanoladder scaffolds.

To identify glial cells, we used a specific marker, glial fibrillary acidic protein (GFAP, Sigma-Aldrich, MO), an intermediate

DOI: 10.1021/acsbiomaterials.7b00981
ACS Biomater. Sci. Eng. 2018, 4, 1037−1045

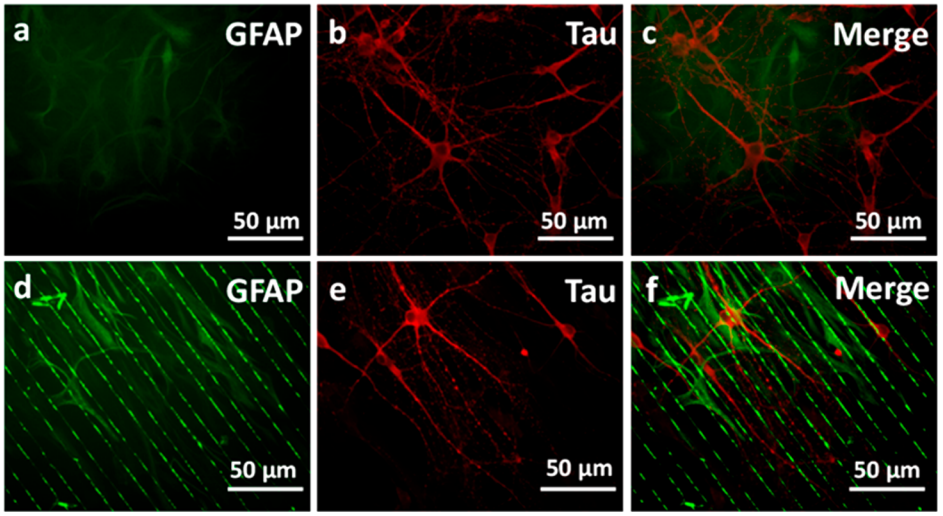

Figure 6. Alignment of glial cells helps directional neuronal regeneration on the nanoladder scaffold. GFAP labeled glial cells (a,d), anti-Tau labeled neurite in the glial cells and embryonic neuron cells coculture (b,e), and merged images (c,f) on the cover glass and nanoladder scaffold, respectively.

filament protein expressed in the glial cell cytoskeleton. We observed a significant expansion of glial cells on the cover glass via immunofluorescence staining, shown in SI Figure S6a,b. The regenerated axon bundle is expected to grow on top of the glial cell layer and was confirmed by SRS imaging through tuning the Z position of the focus lens. As shown in the SRS images in SI Figure S6c,d, there are two layers of cells colocalizing. The cells at the bottom layer were at a spherical shape, which were identified as glial cells, while the elongated cells at the top layer appeared to be neurons.

The SEM images (SI Figure S7a,b) of the culture on the nanoladders further revealed the directional guidance effect of the nanoladder scaffolds to glial and neuron cells. Influenced by the nanoladder, the glial cells attaching to the tip of the nanoprotrusions exhibited a directional and elongated manner of growth (SI Figure S7a). The aligned glial cells further guided the neuronal regeneration along the direction of the nanoladders in the organotypic tissue slice cultures (SI Figure S7b).

To confirm the above observations, we studied the interaction between glial cell and primary neuron cocultured on the nanoladder scaffold. To prepare the coculture, glial cells from P3-5 neonatal rat brain were first seeded onto either cover glass or nanoladder scaffold. Different from the cell cultures discussed above, we did not coat the substrates with Poly-D-Lysine for coculture, therefore neurons are expected to grow on the areas where glial cells are present. After 1 week in culture, spinal cord neurons were then seeded on top of the existing glial cell layer. We stained for anti-Tau (red) and GFAP (green) to identify axons and glial cells, respectively. In the control group shown in Figure 6a–c, both glial and neuron cells grew randomly without preferred orientation. On the contrary, in the nanoladder group, the GFAP positive cells, possibly astrocytes, were partially oriented by the nanoladder scaffolds (Figure 6d), which guided the neuron cells on top to follow the direction of nanoladder. Co-localization of orientation of the nanoladders, oriented glial cells, and axons was observed in Figure 6f. Together with the previous observations from the organotypic tissue slices culture, the coculture system indicates that the nanoladder scaffolds can guide the directional growth of the glial cells, which further promotes the regeneration of neuronal axons."

4. DISCUSSION

In this work, we developed a nanoladder scaffold to mimic the native organization of axon bundles to guide directional neurite outgrowth and functional reconnection over a distance of 1 mm. We have demonstrated significant neurite directional elongation in parallel with the nanoladder direction via culturing embryonic neuron cells on the nanoladder scaffolds. We further showed morphological and functional reconnections between a pair of the slices placed over 1 mm by introducing organotypic spinal cord tissue slices as the injury model. We also investigated the influence of nanoladder scaffolds on non-neuronal cells, such as glial cells. Our results indicate that nanoladder scaffolds enable directional outgrowth of the glial cells in the organotypic spinal cord slices as well as the glial and neuron coculture.

We note that various neuron-material interfaces have been reported. The majority of these platforms can be specified into two categories: micron-scale[20,25] and nanoscale structures.[26] Microstructures, such as grooves, pillars, posts, pyramids, and isotropically etched cavities, in the range of 1 to 200 μm were utilized for directing neural growth.[27] Nanostructures, such as nanotubes, nanopillars, and nanowires, were reported to restore the native extracellular matrix organizations to facilitate neuronal regeneration after injuries.[28−30] Here, we show for the first time that directional axonal outgrowth and regeneration achieved on a single scaffold using segregated organotypic spinal tissue slices placed over 1 mm apart. Such distance is relevant to many currently used spinal cord injury models.[31] The ability to guide directional regeneration in the millimeter scale promises nanoladder with potential clinical applications toward spinal cord injury treatment. We attribute this capability to the unique integration of two structures on our nanoladder scaffold, which are the micrometer-wide stripes that guide the growth of neurons and the nanometer-scale protrusions that promote the formation of neurites.

We also note that nanotubes have been successfully used to facilitate nerve electric signaling in spinal cord.[32] The multiwall carbon nanotubes were used independently and integrated with other materials to help stimulate neuronal recovery.[33] In particular, Ballerini and co-workers demonstrated the reformation of neural networks on the nanotube platforms to support

DOI: 10.1021/acsbiomaterials.7b00981
ACS Biomater. Sci. Eng. 2018, 4, 1037−1045

the reconnection of segregated spinal cord segments.[11] The authors also commented that the conductivity of the materials can enhance the electrophysiological activities of the injured tissue and create artificial bridges to restore electrical connectivity.[30] Notably, such connectivity is not cell specific. More importantly, the use of conductive carbon nanomaterial matrix may introduce unnecessary spontaneous activities and electric connections to influence nerve activities, which could potentially cause major side effects such as chronic pain. The nonconductivity of our SiO_2-based nanoladder scaffold ensures that all electric connectivity is truly formed by cell-specific synaptic connections.

Another advantage of SiO_2 is its biocompatibility. Unlike silicone, stainless-steel elements, or platinum−iridium electrodes that are ultimately rejected by the human organism,[34] SiO_2 has been widely used as drug delivery vehicles *in vivo*, which shows high compliance with the cells and tissues.[35] With established surface chemistry, SiO_2 can be functionalized with growth factor and extracellular matrix molecules to further enhance the facilitating effect of the neuronal outgrowth.[36] Compared to samples prepared on nontransparent silicon wafers,[8,9] neurons or tissues can be directly cultured on the SiO_2-based nanoladder substrates for live cell optical imaging. Such volatility opens up the potential of using the nanoladder scaffold as a platform to understand cell−nanotopography interactions.

Finally, our study provides a foundation for developing 3D nanoladder structure for spinal cord injury repair *in vivo*. It was reported that 3D interconnected and addressable nanoelectronic networks can be fabricated from ordered 2D nanowire nanoelectronic precursors through conventional lithography.[37,38] Since the current clinical treatment of SCI is limited by the regeneration of the ordered 3D alignment of neuronal network to regain functional recoveries, such nanoladder scaffold can be coupled with other soft materials, such as hydrogels and polymer materials, to fabricate injectable 3D structures.[39−41] Further study along this direction promises broad applications in clinical spinal cord injury treatment and brain-computer interface development.

5. CONCLUSIONS

A nanoladder scaffold, composed of parallel aligned micrometer-wide stripes and nanoprotrusions on the stripe surface, was demonstrated for directional outgrowth of neurons. Embryonic neurons cultured on the surface of the nanoladder scaffolds established a directional elongated outgrowth. The averaged neurite length of the nanoladder group is 1.7 times longer than that of the control group. In total, 79.12% of the neurites from the neurons cultured on nanoladder scaffolds were distributed within the angle in the range of −30° to 30°, toward the orientation of the nanoladder scaffolds. The efficacy of nanoladder scaffolds in facilitating neuron regeneration was confirmed by using organotypic spinal cord slices as an *ex vivo* injury model. Enhanced morphological and functional reconnections were obtained for pairs of the spinal cord tissue slices placed in the distance of 1 to 1.5 mm along the nanoladder scaffolds. Further imaging studies revealed that directional growth of glial cells preguided the regeneration process. In all, the nanoladder scaffold presented in this work offers a novel platform for studies of neuronal development, neuro−glial interaction, and has the potential for functional restoration after spinal cord injury.

■ ASSOCIATED CONTENT

Supporting Information

The Supporting Information is available free of charge on the ACS Publications website at DOI: 10.1021/acsbiomaterials.7b00981.

SEM images of embryonic neuron cultured on nanoprotrusions; fabrication process; pattern design and SEM images of neurons cultured on micronstripe; cross-sectional SEM images of nanoladder; electrophysiology experimental setting and LFP curves; IF and SRS images of spinal cord tissue slices; and SEM images of spinal cord tissue slices cultured on nanoladder (PDF)

■ AUTHOR INFORMATION

Corresponding Authors

*E-mail: cheyang@bu.edu.
*E-mail: xu26@iupui.edu.
*E-mail: jxcheng@bu.edu.

ORCID

Yimin Huang: 0000-0001-9739-3629
Ji-Xin Cheng: 0000-0002-5607-6683
Chen Yang: 0000-0001-9454-847X

Author Contributions

¶(Y.H., Y.J.) These authors contributed equally to this work.

Notes

The authors declare no competing financial interest.

■ ACKNOWLEDGMENTS

This work is partially supported by a W. M. Keck Foundation Science & Engineering Grant and Boston University Start-up funds.

■ REFERENCES

(1) Schmidt, C. E.; Leach, J. B. Neural tissue engineering: strategies for repair and regeneration. *Annu. Rev. Biomed. Eng.* **2003**, *5*, 293−347.

(2) Sekiya, T.; Holley, M. C.; Hashido, K.; Ono, K.; Shimomura, K.; Horie, R. T.; Hamaguchi, K.; Yoshida, A.; Sakamoto, T.; Ito, J. Cells transplanted onto the surface of the glial scar reveal hidden potential for functional neural regeneration. *Proc. Natl. Acad. Sci. U. S. A.* **2015**, *112* (26), E3431−40.

(3) Liu, C.; Huang, Y.; Pang, M.; Yang, Y.; Li, S.; Liu, L.; Shu, T.; Zhou, W.; Wang, X.; Rong, L.; Liu, B. Tissue-engineered regeneration of completely transected spinal cord using induced neural stem cells and gelatin-electrospun poly (lactide-co-glycolide)/polyethylene glycol scaffolds. *PLoS One* **2015**, *10* (3), e0117709.

(4) Tator, C. H.; Fehlings, M. G. Review of the secondary injury theory of acute spinal cord trauma with emphasis on vascular mechanisms. *J. Neurosurg.* **1991**, *75* (1), 15−26.

(5) Silva, N. A.; Sousa, N.; Reis, R. L.; Salgado, A. J. From basics to clinical: a comprehensive review on spinal cord injury. *Prog. Neurobiol.* **2014**, *114*, 25−57.

(6) Xie, J.; Liu, W.; MacEwan, M. R.; Bridgman, P. C.; Xia, Y. Neurite outgrowth on electrospun nanofibers with uniaxial alignment: the effects of fiber density, surface coating, and supporting substrate. *ACS Nano* **2014**, *8* (2), 1878−85.

(7) Loesberg, W. A.; te Riet, J.; van Delft, F. C.; Schon, P.; Figdor, C. G.; Speller, S.; van Loon, J. J.; Walboomers, X. F.; Jansen, J. A. The threshold at which substrate nanogroove dimensions may influence fibroblast alignment and adhesion. *Biomaterials* **2007**, *28* (27), 3944−51.

(8) Xie, C.; Hanson, L.; Xie, W.; Lin, Z.; Cui, B.; Cui, Y. Noninvasive neuron pinning with nanopillar arrays. *Nano Lett.* **2010**, *10* (10), 4020−4.

DOI: 10.1021/acsbiomaterials.7b00981
ACS Biomater. Sci. Eng. 2018, 4, 1037−1045

(9) Kang, K.; Park, Y. S.; Park, M.; Jang, M. J.; Kim, S. M.; Lee, J.; Choi, J. Y.; Jung, D. H.; Chang, Y. T.; Yoon, M. H.; Lee, J. S.; Nam, Y.; Choi, I. S. Axon-First Neuritogenesis on Vertical Nanowires. *Nano Lett.* **2016**, *16* (1), 675−80.
(10) Lovat, V.; Pantarotto, D.; Lagostena, L.; Cacciari, B.; Grandolfo, M.; Righi, M.; Spalluto, G.; Prato, M.; Ballerini, L. Carbon nanotube substrates boost neuronal electrical signaling. *Nano Lett.* **2005**, *5* (6), 1107−10.
(11) Usmani, S.; Aurand, E. R.; Medelin, M.; Fabbro, A.; Scaini, D.; Laishram, J.; Rosselli, F. B.; Ansuini, A.; Zoccolan, D.; Scarselli, M.; De Crescenzi, M.; Bosi, S.; Prato, M.; Ballerini, L. 3D meshes of carbon nanotubes guide functional reconnection of segregated spinal explants. *Sci. Adv.* **2016**, *2* (7), e1600087.
(12) Teng, Y. D.; Lavik, E. B.; Qu, X.; Park, K. I.; Ourednik, J.; Zurakowski, D.; Langer, R.; Snyder, E. Y. Functional recovery following traumatic spinal cord injury mediated by a unique polymer scaffold seeded with neural stem cells. *Proc. Natl. Acad. Sci. U. S. A.* **2002**, *99* (5), 3024−9.
(13) Ichiki, T.; Sugiyama, Y.; Ujiie, T.; Horiike, Y. Deep dry etching of borosilicate glass using fluorine-based high-density plasmas for micrbelectromechanical system fabrication. *J. Vac. Sci. Technol., B: Microelectron. Process. Phenom.* **2003**, *21*, 2188−2192.
(14) Park, J. H.; Lee, N. E.; Lee, J.; Park, J. S.; Park, H. D. Deep dry etching of borosilicate glass using SF6 and SF6/Ar inductively coupled plasmas. *Microelectron. Eng.* **2005**, *82*, 119−128.
(15) Gerardo-Nava, J.; Hodde, D.; Katona, I.; Bozkurt, A.; Grehl, T.; Steinbusch, H. W. M.; Weis, J.; Brook, G. A. Spinal cord organotypic slice cultures for the study of regenerating motor axon interactions with 3D scaffolds. *Biomaterials* **2014**, *35*, 4288−4296.
(16) Lee, H. J.; Zhang, D.; Jiang, Y.; Wu, X.; Shih, P. Y.; Liao, C. S.; Bungart, B.; Xu, X. M.; Drenan, R.; Bartlett, E.; Cheng, J. X. Label-Free Vibrational Spectroscopic Imaging of Neuronal Membrane Potential. *J. Phys. Chem. Lett.* **2017**, *8*, 1932−1936.
(17) Zelniker, E. E.; Bradley, A. P.; Castner, J. E.; Chenery, H. J.; Copland, D. A.; Silburn, P. A. Estimation of neuronal firing rates with the three-state biological point process model. *J. Neurosci. Methods* **2008**, *174*, 281−91.
(18) Kwon, B. K.; Liu, J.; Messerer, C.; Kobayashi, N. R.; McGraw, J.; Oschipok, L.; Tetzlaff, W. Survival and regeneration of rubrospinal neurons 1 year after spinal cord injury. *Proc. Natl. Acad. Sci. U. S. A.* **2002**, *99*, 3246−51.
(19) Lin, T.; Ramadurgam, S.; Liao, C. S.; Zi, Y.; Yang, C. Fabrication of Sub-25 nm Diameter GaSb Nanopillar Arrays by Nanoscale Self-Mask Effect. *Nano Lett.* **2015**, *15*, 4993−5000.
(20) Fozdar, D. Y.; Lee, J. Y.; Schmidt, C. E.; Chen, S. Selective axonal growth of embryonic hippocampal neurons according to topographic features of various sizes and shapes. *Int. J. Nanomed.* **2010**, *6*, 45−57.
(21) Ravikumar, M.; Jain, S.; Miller, R. H.; Capadona, J. R.; Selkirk, S. M. An organotypic spinal cord slice culture model to quantify neurodegeneration. *J. Neurosci. Methods* **2012**, *211*, 280−8.
(22) Heidemann, M.; Streit, J.; Tscherter, A. Functional regeneration of intraspinal connections in a new in vitro model. *Neuroscience* **2014**, *262*, 40−52.
(23) Tysseling-Mattiace, V. M.; Sahni, V.; Niece, K. L.; Birch, D.; Czeisler, C.; Fehlings, M. G.; Stupp, S. I.; Kessler, J. A. Self-assembling nanofibers inhibit glial scar formation and promote axon elongation after spinal cord injury. *J. Neurosci.* **2008**, *28*, 3814−23.
(24) Wu, W.; Wu, W.; Zou, J.; Shi, F.; Yang, S.; Liu, Y.; Lu, P.; Ma, Z.; Zhu, H.; Xu, X. M. Axonal and glial responses to a mid-thoracic spinal cord hemisection in the Macaca fascicularis monkey. *J. Neurotraum* **2013**, *30* (10), 826−39.
(25) Li, N. Z.; Folch, A. Integration of topographical and biochemical cues by axons during growth on microfabricated 3-D substrates. *Exp. Cell Res.* **2005**, *311*, 307−316.
(26) Pan, F.; Zhang, M.; Wu, G. M.; Lai, Y. K.; Greber, B.; Scholer, H. R.; Chi, L. F. Topographic effect on human induced pluripotent stem cells differentiation towards neuronal lineage. *Biomaterials* **2013**, *34* (33), 8131−8139.
(27) Nikkhah, M.; Edalat, F.; Manoucheri, S.; Khademhosseini, A. Engineering microscale topographies to control the cell-substrate interface. *Biomaterials* **2012**, *33*, 5230−46.
(28) Kotov, N. A.; Winter, J. O.; Clements, I. P.; Jan, E.; Timko, B. P.; Campidelli, S.; Pathak, S.; Mazzatenta, A.; Lieber, C. M.; Prato, M.; Bellamkonda, R. V.; Silva, G. A.; Kam, N. W. S.; Patolsky, F.; Ballerini, L. Nanomaterials for Neural Interfaces. *Adv. Mater.* **2009**, *21*, 3970−4004.
(29) Fabbro, A.; Bosi, S.; Ballerini, L.; Prato, M. Carbon nanotubes: artificial nanomaterials to engineer single neurons and neuronal networks. *ACS Chem. Neurosci.* **2012**, *3*, 611−8.
(30) Marchesan, S.; Ballerini, L.; Prato, M. Nanomaterials for stimulating nerve growth. *Science* **2017**, *356*, 1010−1011.
(31) Cheriyan, T.; Ryan, D. J.; Weinreb, J. H.; Cheriyan, J.; Paul, J. C.; Lafage, V.; Kirsch, T.; Errico, T. J. Spinal cord injury models: a review. *Spinal Cord* **2014**, *52*, 588−95.
(32) Cellot, G.; Cilia, E.; Cipollone, S.; Rancic, V.; Sucapane, A.; Giordani, S.; Gambazzi, L.; Markram, H.; Grandolfo, M.; Scaini, D.; Gelain, F.; Casalis, L.; Prato, M.; Giugliano, M.; Ballerini, L. Carbon nanotubes might improve neuronal performance by favouring electrical shortcuts. *Nat. Nanotechnol.* **2009**, *4*, 126−33.
(33) Bosi, S.; Rauti, R.; Laishram, J.; Turco, A.; Lonardoni, D.; Nieus, T.; Prato, M.; Scaini, D.; Ballerini, L. From 2D to 3D: novel nanostructured scaffolds to investigate signalling in reconstructed neuronal networks. *Sci. Rep.* **2015**, *5*, 9562−73.
(34) Lacour, S. P.; Courtine, G.; Guck, J. Materials and technologies for soft implantable neuroprostheses. *Nat. Rev. Mater.* **2016**, *1*, 16063−16077.
(35) Slowing, I. I.; Trewyn, B. G.; Giri, S.; Lin, V. S. Y. Mesoporous silica nanoparticles for drug delivery and biosensing applications. *Adv. Funct. Mater.* **2007**, *17*, 1225−1236.
(36) Grimpe, B.; Dong, S.; Doller, C.; Temple, K.; Malouf, A. T.; Silver, J. The critical role of basement membrane-independent laminin gamma 1 chain during axon regeneration in the CNS. *J. Neurosci.* **2002**, *22*, 3144−3160.
(37) Li, J.; Zhang, J.; Gao, W.; Huang, G.; Di, Z.; Liu, R.; Wang, J.; Mei, Y. Dry-released nanotubes and nanoengines by particle-assisted rolling. *Adv. Mater.* **2013**, *25*, 3715−21.
(38) Liu, J.; Xie, C.; Dai, X.; Jin, L.; Zhou, W.; Lieber, C. M. Multifunctional three-dimensional macroporous nanoelectronic networks for smart materials. *Proc. Natl. Acad. Sci. U. S. A.* **2013**, *110*, 6694−9.
(39) Bae, W. G.; Kim, J.; Choung, Y. H.; Chung, Y.; Suh, K. Y.; Pang, C.; Chung, J. H.; Jeong, H. E. Bio-inspired configurable multiscale extracellular matrix-like structures for functional alignment and guided orientation of cells. *Biomaterials* **2015**, *69*, 158−64.
(40) Perale, G.; Rossi, F.; Sundstrom, E.; Bacchiega, S.; Masi, M.; Forloni, G.; Veglianese, P. Hydrogels in spinal cord injury repair strategies. *ACS Chem. Neurosci.* **2011**, *2*, 336−45.
(41) Gomes, E. D.; Mendes, S. S.; Leite-Almeida, H.; Gimble, J. M.; Tam, R. Y.; Shoichet, M. S.; Sousa, N.; Silva, N. A.; Salgado, A. J. Combination of a peptide-modified gellan gum hydrogel with cell therapy in a lumbar spinal cord injury animal model. *Biomaterials* **2016**, *105*, 38−51.

DOI: 10.1021/acsbiomaterials.7b00981
ACS Biomater. Sci. Eng. 2018, 4, 1037−1045